RESEARCH ARTICLE

Seismic Response of Pile Foundation at Wolaita Sodo Converter Station

H.A. Abegaze, H. F.Gebregziabher*
Addis Ababa Institute of Technology, Addis Ababa University,
King George VI St., Addis Ababa, Ethiopia

ABSTRACT: This paper is aimed at analyzing the effects of seismic load on piles supporting the electric transmission towers erected between Ethiopia and Kenya. Due to the significance of the project, failure of the foundations shall be avoided and analyzing the lateral response of piles is crucial. To carry out the dynamic analyses, ground motion analyses were executed and a peak ground acceleration of 0.13 g has been obtained from seismic hazard analysis for design basis earthquake. Acceleration-time history data has been obtained from Pacific Earthquake Engineering Research Center ground motion database. Three dimensional finite element analyses were performed to study the response of a single pile under earthquake loading by incorporating infinite element boundary condition to simulate damping. The non-linear Finite Element Analyses performed by modeling the soil using elasto-plastic material model of the Mohr-Coulomb failure criteria indicated that the calculated maximum deformations of the unreinforced pile section are not within recommended limits of the literature, and the use of 0.6 m diameter pile calls for further detailed analyses.

KEYWORDS: Probabilistic Seismic Hazard Analysis; Acceleration Time History; Pile Foundation; Three Dimensional Finite Element Analysis; Dynamic Response.

https://doi.org/10.29294/IJASE.10.1.2023.3246-3258 **©2023 Mahendrapublications.com, All rights reserved**

INTRODUCTION

Transmission tower is an important part of power transmission, which provides a safe and reliable operation of the electric power network. The failure of a power transmission tower under seismic actions will affect the supply of electricity, causing huge economic losses and secondary disasters. When making the design of transmission tower, the major loads considered are static load, wind load, bolt load; while the effects of seismic load are rarely considered [1]. Collapse of transmission towers is common during an earthquake. In the United States, the Landers earthquake in 1992 and the Northridge earthquake severely damaged the transmission system [2]. The 1955 Kobe earthquake in Japan resulted in the destruction of large number of transmission towers where the major failures were subsidence of the foundation and tilting of the tower [3]. The 1999 Chi-Chi earthquake in Taiwan resulted in collapse and distortion on of a large area of a tower structure [4]. During the 2008 Wenchuan earthquake, more than 20 towers of the 110kV transmission line collapsed. Surveys show that most damages of transmission towers occur at the foundation of the structure [5].

Ethiopia is susceptible to two types of seismic hazards; namely, earthquake and volcanic eruptions. [6] cited EM-DAT database that there were a total of seven major earthquakes between 1900 and 2013, killing a total of 24 people, affecting 585 people and causing more than 7 million US$ economic loses. The significant ones are the 1961 Kara Kore earthquake (M=7), the 1969 Sardo earthquake (M=6.4), the 1983 Wendo Genet earthquake, the 1985 Langano earthquake and the 1989 Dobigraben earthquake (M=6.2); some of which were fatal [7].

Most earthquakes affect tens of square kilometers while the severest can destroy areas of 2500 km^2 or more [7]. The converter station is located near the edge of the western plateau of the Main Ethiopian Rift (MER), very close to the foot of Mt. Damota from the western side. Thus, performing dynamic analysis for the pile foundation of the electric transmission tower is very important.

The response of a pile subjected to seismic excitation depends on the pile itself, mechanical

**Corresponding Author: henol.fikre@aait.edu.et*
Received: 10.06.2023 **Accepted:** 27.07.2023 **Published on**: 25.08.2023

properties of the surrounding soil, the interaction between superstructure, pile, and soil and the seismic input. The foundation pile under investigation is exposed to kinematic loading and inertial loading due to earthquake. The deformation of the pile is assumed to be prevailing because of the stiffness difference between the soil and the pile. Secondly, inertial loadings are induced in the piles because of the accelerations generated within the structure by earthquake.

Consideration is generally confined to lateral inertial forces and moments, which are assumed to be applied at the pile heads [8]. Novak[9] used the generalized Winkler model to simulate the dynamic soil-pile interaction system by employing linear elastic interaction between the two materials. The analytical approach is used establish the dimensionless parameters of the problem and obtain closed-form formulas for pile stiffness and damping. Bentley & Naggar [10] studied the effects of kinematic interaction on the input motion at the foundation level. They included pile-soil separation, slippage, soil plasticity, and 3-D wave propagation. [11] used a 3D finite element model to obtain the pile response under seismic excitation and a load applied to the pile cap and column base, with consideration of the nonlinearity effects of the soil and pile-soil interaction in the dynamic behavior of a single pile and pile groups. Dongmei &Truman, [12] used a 3D finite element model to compute seismic response of a soil-pile foundation system, nonlinear analyses are performed in the time domain and an infinite element boundary condition is used to simulate radiation damping. Liuet al., [5] used finite element method to compute the response of pile-soil-transmission tower under seismic load by employing time history analysis. Based on the experience from the previous studies, the current research has also employed the finite element software ABAQUS for the full dynamic analyses after determining the seismic hazard analyses. The research has thus focused on the investigation of the effects of seismic load on piles supporting the electric transmission towers between Ethiopia and Kenya.

2. MATERIALS AND METHODS

2.1. Seismic Hazard Analysis

The electric transmission tower converter station under consideration is located between 6.9°-7° E and 37.72°-38° N, at the edge the western plateau of the Main Ethiopian Rift (MER) that is susceptible to seismic actions. To carry out the dynamic analysis, acceleration time history record is required although there is no recorded data in Ethiopia [13]. Probabilistic seismic hazard analysis and deaggregation have been performed for the dynamic analysis by using time history from previous earthquake database.

2.1.1. Probabilistic Seismic Hazard Analysis

Earthquake size directly related to the amount of energy released in them. The Gutenberg-Richter magnitude recurrence model better represents earthquake magnitude recurrence [14] is given by Equation 1.

$$\log(\lambda_m) = a - bM \quad (1)$$

where λ_m is the rate of earthquakes with magnitudes greater than M. The constant a and b values are estimated from historical observations. Ayele [15] gave a constant b value of 0.77, earthquake magnitude value of 7.2 and the rate of earthquake 0.593.

In Chiou and Youngs [19] attenuation models, the effect of depth of faulting included the depth-to-top of rupture and down-d0ip rupture width shown in Figure 1. This depth is measured to the top of the specific earthquake rupture by the empirical equation of [16]. The down-dip rupture width is determined by using the logarithmic relationships [17]. Style of faulting is a useful parameter to include in ground motion prediction equation. There are three general types of styles of faulting; namely reverse, strike-slip, and normal types. The PGA calculation has been done using normal slip faults because it is the dominant fault mechanism [18].

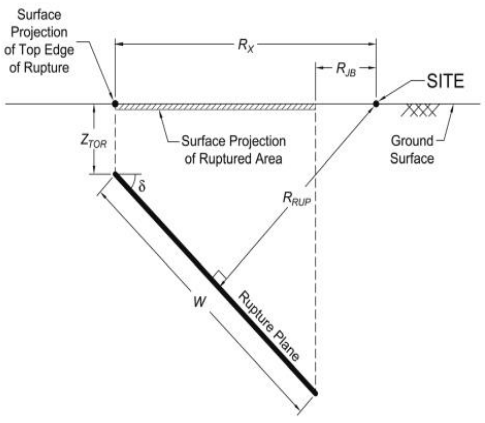

Figure 1: Illustration of earthquake source and distance measures using a vertical cross section through a fault rupture plane.

In Chiou and Young attenuation models, several distance definition have been used such (R_{rup}), the shortest horizontal distance to the surface of projection of the rupture area (also referred to as Joyner-Boore distance),R_{JB}; the horizontal distance to surface projection of the top of rupture plane, measured perpendicular to the fault strike, R_x. Both R_{JB} and R_X are used to model the attenuation of hanging wall effects. The distance to the fault is defined to be reliable with the specific attenuation relationship used to calculate the ground motion.

The amplitude of the ground motion depends on the properties of the material through which waves propagate. Site classifications are based on the shear wave velocity in the top 30 m primary characteristic in the NGA models. Chiou and Young [15] add sediment thickness as a second site parameter. It defines the depth to a material (bedrock) with shear-wave velocity, v_s of 1 km/sec or greater.

as the closest distance to the rupture plane

2.1.2. Ground Motion Prediction Equations

Ground motion prediction equations are used to measure ground-motion intensity, such as peak ground acceleration and spectral acceleration at the individual vibration period, including the characteristics of source, path and site parameters. Ground motion prediction equations are constructed by statistical regression analysis of many strong motion records. These ground motion models are developed for three distinct different tectonic zones: shallow crustal earthquakes, subduction zones, and stable continental regions. Chiou and Young ground motion model was developed from shallow crustal earthquakes [19]. The ground motion model is represented in Equations 2 and 3.

$$\ln\left(y_{ref_{ij}}\right) = c_1 + [c_{1a}F_{RVi} + c_{1b}F_{NMi} + c_7(Z_{TORi} - 4)](1 - AS_i) + [c_{10} + c_{7a}(Z_{TORi} - 4)]AS_i + c_2(\mathbf{M}_i - 6) + \frac{c_2 - c_3}{c_n}\ln\left(1 + e^{c_n(c_M - \mathbf{M}_i)}\right) + c_4\ln\left[R_{RUPij} + \cosh\{c_6\max(\mathbf{M}_i - c_{HM}, 0)\}\right] + (c_{4a} - c_4)\ln\left(\sqrt{R^2{}_{RUPij} + c^2{}_{RB}}\right) + \left\{c_{\gamma 1} + \frac{c_{\gamma 2}}{\cosh\left[\max\left(\mathbf{M}_i - c_{\gamma 3}\right)\right]}\right\}R_{RUPij} + c_9F_{HWij}\tanh\left(\frac{R_{Xij}\cos^2\delta_i}{c_{9a}}\right)\left\{1 - \frac{\sqrt{R^2{}_{JBij} + Z^2{}_{TORi}}}{R_{RUPij}+0.001}\right\} \quad (2)$$

$$\ln(y_{ij}) = \ln\left(y_{ref_{ij}}\right) + \phi_1 \cdot \min\left(\ln\left(\frac{V_{S30j}}{1130}\right), 0\right) + \phi_2\left\{e^{\phi_3(\min(V_{S30j},\ 1130) - 360)} - e^{\phi_3(1130 - 360)}\right\}\ln\left(\frac{y_{ref_{ij}}e^{\eta_i} + \phi_4}{\phi_4}\right) + \phi_5\left(1 - \frac{1}{\cosh[\phi_6 \cdot \max(0, Z_{1.0} - \phi_7)]}\right) + \frac{\phi_8}{\cosh[0.15 \cdot \max(0, Z_{1.0} - 15)]} + \eta_i + \varepsilon_{ij} \quad (3)$$

where,M Moment magnitude

R_{RUP} The closest distance to the rupture plane (km)

R_X Site coordinate (km) measured perpendicular to the fault strike from the surface projection of the up-dip edge of the fault rupture, with the down-dip direction being positive.

F_{HW} Hanging-wall flag: 1 for $R_X \geq 0$ and 0 for $R_X < 0$

δ Fault dip angle

F_{RV} Reverse faulting flag: 1 for $30° \leq \lambda \leq 150°$ (combined reverse and reverse oblique), 0 otherwise; λ is the rake angle

F_{NM} Normal faulting flag: 1 for $-120° \leq \lambda \leq -60°$ (excludes normal-oblique), 0 otherwise.

R_{JB} Joyner-Boore distance to the rupture plane (km)

AS Aftershock flag: 1 if the event is an aftershock, 0 otherwise

V_{S30} Average shear wave velocity in the top 30 m (m/s)

Z_{TOR} Depth to top of rupture (km)

$Z_{1.0}$ Depth to shear wave velocity of 1.0 km/s (m).

Martin & Perez [20] used log normal distribution to model engineering data. Huyse et al., [21] demonstrated that 10^{-6} is the smallest annual probability exceedance for low

probability ground motions by using lognormal distribution. In this paper, lognormal

The annual rate of exceedance$\lambda(PGA > x)$ computed by the sum of the rates of PGA > x from each source to compute hazard curve is shown in Figure 2.The probabilistic seismic hazard analysis (PSHA) resulted in a horizontal PGA of 0.13g for design basis earthquake. The distribution exceedance varying from 0.05 to 0.8 g with intervals of 0.05has been generated.

PGA value of the design basis earthquake is within the range of recommendations stated on the seismic hazard map of Ethiopia for return period of 475 years by [22] which is in the range between 0.1g and 0.16g as shown in Figure 3.

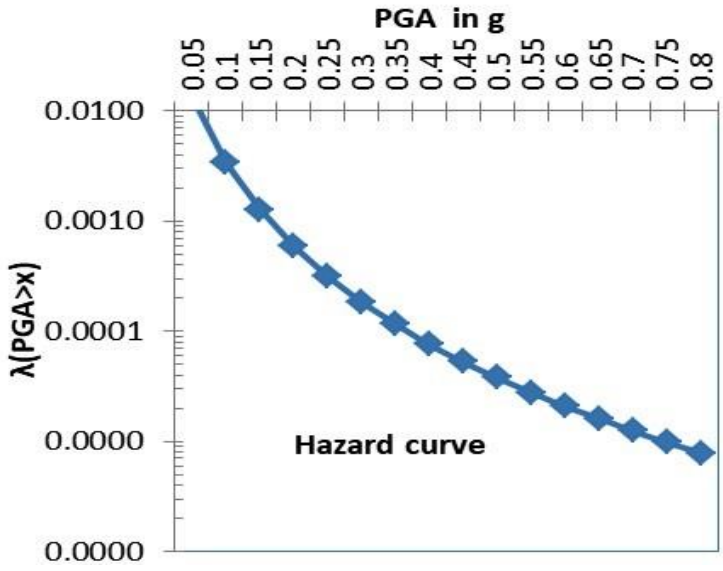

Figure 2.Hazard Curve for the specific site

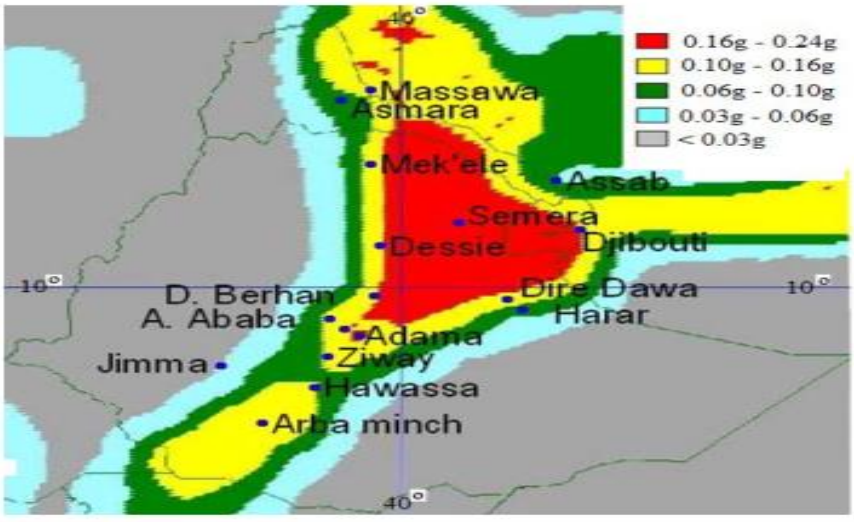

Figure 3: Seismic hazard map of Ethiopia based on the GSHAP data for a return period of 475 years [22]

2.1.3 Deaggregation

The hazard curve gives the combined effect of all magnitudes and distances on the probability of exceeding a given ground motion level. To provide insight into what events are the most significant contributions to the seismic hazard to determine the maximum considered earthquake (PGA), the hazard curve is broken down into its contributions from several sources for each related magnitude and source-to-site distance; which is the process of deaggregation.

Deaggregation identifies the source, distance, and ground motion percentiles that contribute most strongly to the computed hazard. Deaggregation is obtained by dividing the total

hazard contributions based on distance and magnitude for the rate of an earthquake by the rate of all earthquakes [23,24]. The most common form of deaggregation is a two-dimensional (2D) deaggregation in magnitude and distance bins. In this method, the magnitude range is discretized within an equal space of 0.1. The deaggregation resulted in the most dominant magnitude of earthquake of 5.5 and 5.7 and source to site distance of 20.23 km and 15.27 km, respectively. This pair of values is considered as the most likely scenario which corresponds to the DBE for the specific site.

2.1.4 Ground Motion Selection

The selection and scaling of earthquake ground motions has a critical role in seismic load definition that will be applied to a structure during dynamic analysis. Since there are no accelerogram records for Ethiopian earthquakes, other records should be adapted, for which ground motion selection is required [25]. Ground motion selection utilizes deaggregation results of magnitude and distance to identify causal events for a given target spectra value associated with an annual rate of exceedance [26].

To select acceleration time history from the database of Pacific Earthquake Engineering Research Center (PEER); the input factors are the pair of most dominant magnitude and distance from the deaggregation calculation, the top 30 m shear velocity and fault mechanism of the specified area. Acceleration time history has been searched for an earthquake magnitude – distance combination range of 5.5-5.7 magnitude and 15-30 km distance. Top 30 m shear wave velocity of 557 m/s has been used from the geotechnical report as an input on PEER ground motion database. The fault type was selected to be normal fault due to its dominance.

Using the above PGA values, "Umbria Marche" earthquake has been selected from the database using the above mentioned inputs to characterize the area. The PGA value of this selected earthquake (0.163g) is used to scale the calculated PGA from PSHA value 0.13g. The scaling factor of the PGA becomes:

$$\frac{0.13}{0.163} = 0.797$$

The most commonly employed ground motion scaling method involves multiplying all of the acceleration values of the time-acceleration pairs by a scalar value. This time domain scaling modifies the amplitude of the accelerations without affecting the frequency content or phasing.

$$Z = 0.8 * 0.797 * 9.81 \ {}^{m}/_{s^2}/_{g} = 6.25$$

The scaled time acceleration histories are shown in Figure 4.

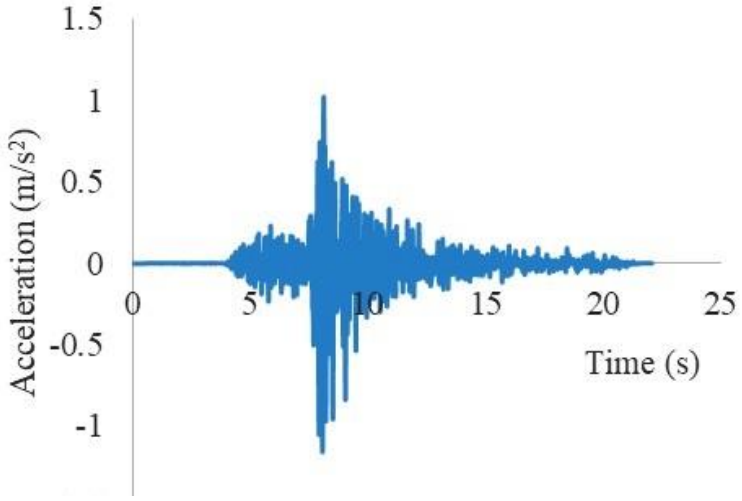

Figure 4: Scaled acceleration time history

2.2 Three-dimensional finite element model

The three dimensional Finite Element Method (FEM) software ABAQUS is used to model the pile- soil system under seismic excitation. The pile and the soil were modeled using linear brick elements with eight-nodes and incompatible modes. A three dimensional

surface to surface contact element was used between the pile and the surrounding soil. Quiet boundaries were used to avoid wave reflection under seismic excitation by employing infinite elements. The quite boundaries do not transmit waves from near field to far-field without reflections.

2.2.1 Soil Geometry and Properties

The multilayered silty clay soil was modeled using Mohr-Coulomb constitutive model, with the soil parameters obtained from the geotechnical investigation report of the project, summarized in Table 2.

2.2.2 Pile Geometry and Properties

The 15 m long concrete made pile is having circular cross sections of 0.6 m and 0.8 m diameters. The linear elastic material parameters of the pile are tabulated below (Table 1).

Table 1: Geometry and properties of pile

No	Parameters	Unit	Value
1	Unit Weight	kN/m^3	25
2	Young's modulus	kPa	30E6
3	Poisson's ratio	[-]	0.15
4	Pile diameter	m	0.6 and 0.8
5	Pile length	m	15
6	Pile head	[-]	Free

Table 2: Soil properties of different layers

	Layer thickness	Unit Weight	Young's Modulus	Poisson's Ratio	Friction Angle	Cohesion	Lateral Earth Pressure Coefficient
Symbol	t	**γ**	E	**ν**	**ϕ'**	c'	K_0
Unit	m	kN/m^3	MPa	[-]	^{o}	kPa	[-]
Layer 1	4.5	17	8	0.3	18	12	0.691
Layer 2	6	19	15	0.3	22	15	0.658
Layer 3	4.5	20	35	0.3	24	20	0.626
Layer 4	15	21	40	0.3	26	25	0.562

Linear brick elements with eight-nodes of incompatible modes (C3D8I) were used to improve the computational time. The soil was assumed to be in dry state to avoid liquefaction problem. The dimensions of the soil shown in Figure 5were adopted from the recommendations of [27]. Material damping in soils was considered to be succeeded mainly through viscous damping. Therefore, traditionally, when computing material damping in soils, mass proportional damping is neglected and damping of the soil is achieved through stiffness proportional material damping. The governing equation of the system is given by:

$$[M]\{u''\}+[C]\{u'\}+[K]\{u\}+\{F(t)\} \qquad (4)$$

where:

$\{u''\}$, $\{u'\}$ and $\{u\}$ are the acceleration, velocity, and displacement respectively.

$[M]$, $[C]$ and $[K]$ are mass, damping, and stiffness matrices, respectively.

$F(t)$ is force function.

The damping matrix [C] = β[K], in which the damping coefficient $\beta = \frac{2\tau}{\omega_o}$, with, ω_0 beeing the predominant circular frequency of loading, and τ is the material damping ratio of soil assumed to be 5 % [10]. Predominant frequency is obtained from a Fourier spectrum drawn for the input wave from the analyzed time history as shown in Figure 6.

2.2.3 Soil-Pile Interface

The contact at the circumferential pile boundary is modeled by defining the surface to surface contact between the pile and the surrounding soil. The pile-soil interaction is defined by tangential and normal contact behavior. Normal contact behavior used hard contact with penalty constraint enforcement method that allows any pressure to be transmitted between surfaces if they are in contact. Regarding the tangential contact, the shear behavior between two surfaces is defined by the Coulomb frictional law. The Coulomb friction model states that two contacting surfaces can carry shear stresses up to a certain magnitude across their interface before they start sliding relative to one another [28]. The Coulomb friction model defines this critical shear stress, at which sliding of the surfaces starts as a fraction of the contact pressure, , between the surface, as given in Equation 5.

$$\tau_{crit} = \mu p \qquad (5)$$

Where τcrit the critical shear stress at contact surface, μ is the coefficient of friction and, is the contact pressure between two surfaces. The friction coefficient was assumed to be isotropic and a value of μ = 0.5 was used.

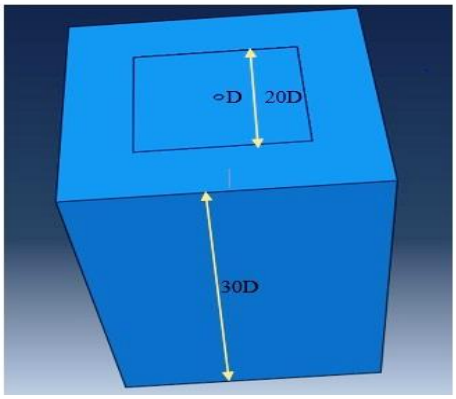

Figure 5: Three dimensional view of the model

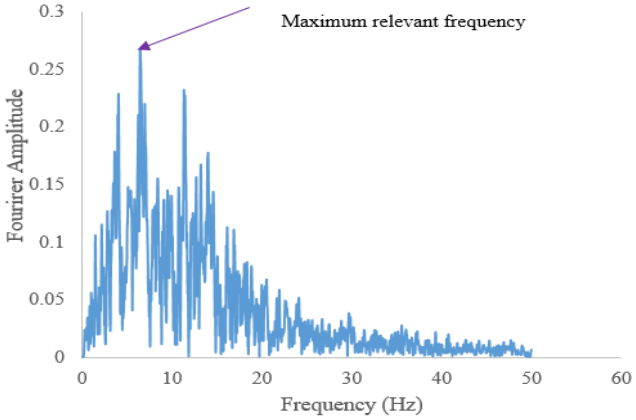

Figure 6: Fourier transformation of the earthquakes

2.2.4 Numerical Accuracy and Stability

The numerical simulation of dynamic Soil-Structure-Interaction (SSI) is controlled by two main parameters. These are the spacing of the nodes of the finite element model *Δh* and the length of the time step *Δt*. assuming that the numerical method converges toward the exact solution as *Δt* and *Δh* approach zero, the desired accuracy of the solution can be obtained as long as sufficient computational resources are available. In order to represent a traveling wave of a given frequency accurately, about 10 nodes per wave length are required. Fewer than 10 nodes can lead to numerical damping as the discretization misses certain peaks of the wave [29]. The value of the highest relevant frequency is 8.5 from Fourier amplitude analysis of input motion but recommended a frequency of 10 Hz to determine the appropriate maximum grid spacing for seismic analysis [29]. Thus, the maximum relevant frequency in this research is on acceptable range as shown Figure 6.

The recommended formula relating grid spacing (Δh), time step of analysis (Δt), smallest wave

velocity of soil medium (v) and the highest relevant frequency (f_{max}) that is present in the model need to be found by performing a Fourier analysis of the input motion as given in equation 6 and 7.

$$\Delta h = \frac{v}{10\, f_{\max}} \tag{6}$$

$$\Delta t = \frac{\Delta h}{v} \tag{7}$$

Where v is the highest wave velocity

The smallest shear wave velocity of 110 m/s obtained from the geotechnical reports has been used in this research.

2.2.5 Element Mesh Size

For nonlinear numerical model of wave propagation problems, the time step Δt has to be limited for two reasons; i.e., accuracy and stability for all modes. If the time step in the finite element analysis is too large, the wave front can reach two consecutive elements at the same moment. This would violate a fundamental property of wave propagation and can lead to instability. The time step, therefore, needs to be limited. In this model, the smallest grid space Δh was 1.29 m and the maximum time step was 0.012 s.

Minimum mesh sizes that give accurate results and remove excessive calculation time and high computer memory requirements should be calculated. Accordingly, the mesh sizes of the finite element calculation resulted in a size of 0.4 m.

2.2.6 Boundary Conditions

The important aspect of boundary conditions on dynamic analysis is to avoid wave reflection. In this paper, the soil was modeled into two regions, near field region consist finite element and far-field region consist infinite element. Infinite elements are used in boundary value problems with unbounded boundaries (infinite medium). During the dynamic analysis, infinite elements will provide "quiet" boundaries at the finite element model boundaries based on the model of [30]. The infinite element is not available in element definition on ABAQUS. Thus, the far-field region is first defined by three–dimensional acoustic elements with 8 node linear brick elements (AC3D8). These AC3D8 elements are then replaced with CIN3D8 elements, 8 noded three-dimensional linear brick elements. The advantage of using a combination of finite and infinite elements is minimizing computational efforts by reducing the volume of elements used in the analyses The infinite element boundaries also serve the purpose of boundary conditions, and no external boundary conditions need to be specified, as stated in the ABAQUS Documentation Manual. Regarding the combination of finite and infinite element near-field region and far-field region is shown in Figure 7a and the finite element discretization is shown in Figure 7b.

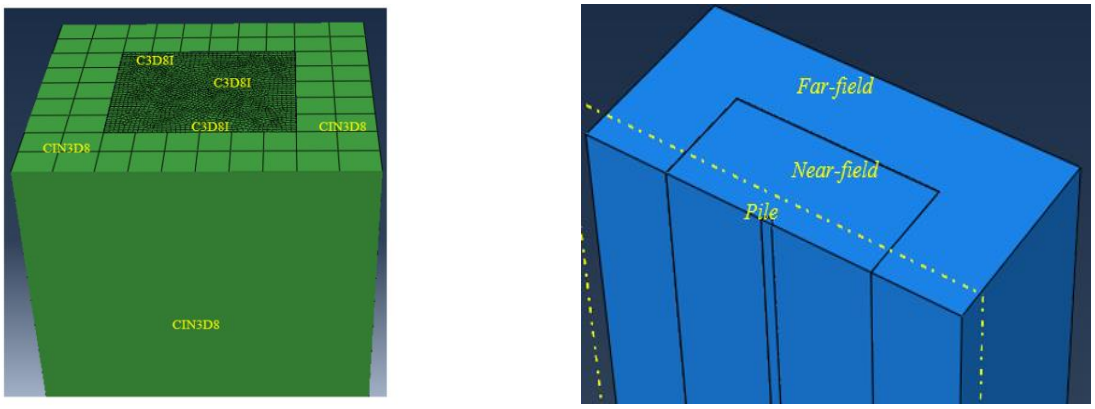

Figure 7: a) Near and far field regions (Half model) b) Finite and infinite element discretization

2.2.7 Loading Steps

The computation of Finite Element Analysis is achieved by the following two loading steps; namely initial and dynamic loading steps. At the initial step of the model, actual in-situ conditions was simulated as an initial loading condition (in-situ stress conditions) before any dynamic or static external load. The geometry and properties of the soil, as well as the boundary conditions and the interaction between the soil and pile are defined in this

step, while the dynamic loading is modeled in a separate load step.

In dynamic analysis, seismic load can be applied either as a displacement, velocity, or acceleration time history at the base of the model. The proposed design horizontal component of seismic acceleration time history corresponding to 475 years return period for Wolaita Sodo site is shown in Figure 4.

Dynamic loading step is applied after geostatic load step. Seismic load is applied at the base of the soil-pile system in the form of acceleration time history after the selection and scaling of the designed time history. The seismic load is applied in both horizontal and vertical directions as the foundation supports a lightweight superstructure. The amplitude of the vertical component is assumed to be 2/3 of the horizontal component (31).

3. RESULTS AND DISCUSSION

To determine the effect of pile size on pile head response, two pile diameters (0.6 m and 0.8 m), which are practically used within the project premises have been considered while keeping pile properties, pile element, mesh sizes, and pile length constant.

3.1 Pile Head Response

Figure 8 shows the pile head response of displacement with dynamic time while Figure 9 shows the acceleration response with dynamic time at pile head for 0.6 m and 0.8 m diameter pile, respectively, the pile head response is studied for both diameters of pile respectively.

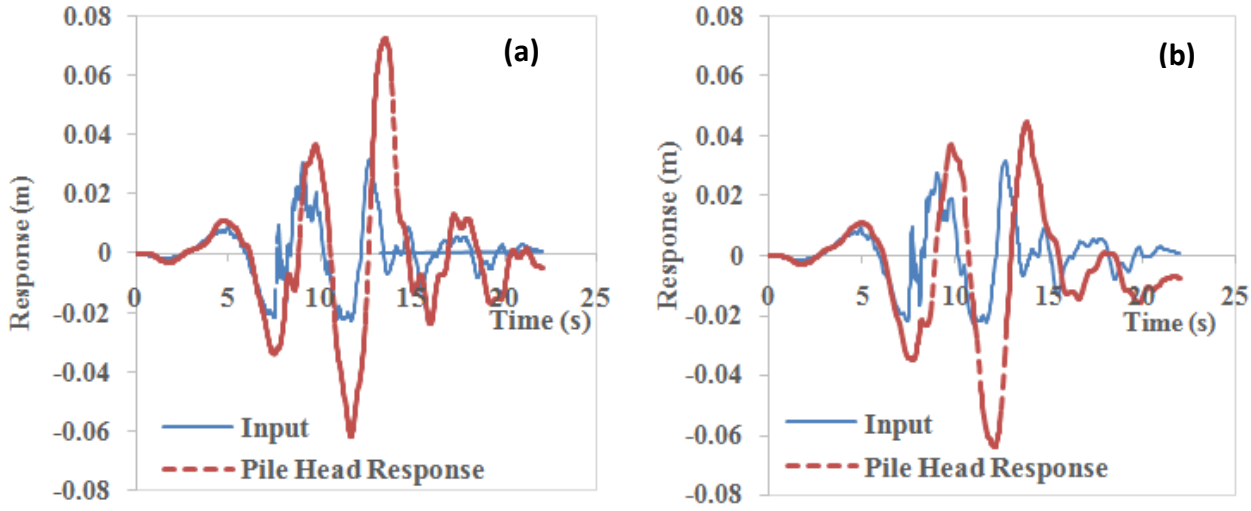

Figure 8: Lateral displacement under kinematic interaction a) diameter 0.6 m b) diameter 0.8 m

It can be observed that the responses of the pile heads follow the pattern of the input acceleration. The input motions were amplified on the response diagrams, both for the acceleration and displacement. The maximum lateral deflections of the piles are 72.02 mm and 63.7 mm for 0.6 m and 0.8 m diameter piles, respectively. Bouzid [32] stated allowable head deflection to be up to 5% of the pile diameter. Accordingly, the obtained pile deflections in this research exceed the acceptable range, the thresholds being 30 and 40 mm for diameter 0.6 m and 0.8 m respectively. This may be attributed to the ignored reinforcement that was not included in the computations to minimize computational efforts.

It can be observed that the responses of the pile heads follow the pattern of the input acceleration. The input motions were amplified on the response diagrams, both for the acceleration and displacement. The maximum lateral deflections of the piles are 72.02 mm and 63.7 mm for 0.6 m and 0.8 m diameter piles, respectively. Bouzid [32] stated allowable head deflection to be up to 5% of the pile diameter. Accordingly, the obtained pile deflections in this research exceed the acceptable range, the thresholds being 30 and 40 mm for diameter 0.6 m and 0.8 m respectively. This may be attributed to the ignored reinforcement that was not included in the computations to minimize computational efforts.

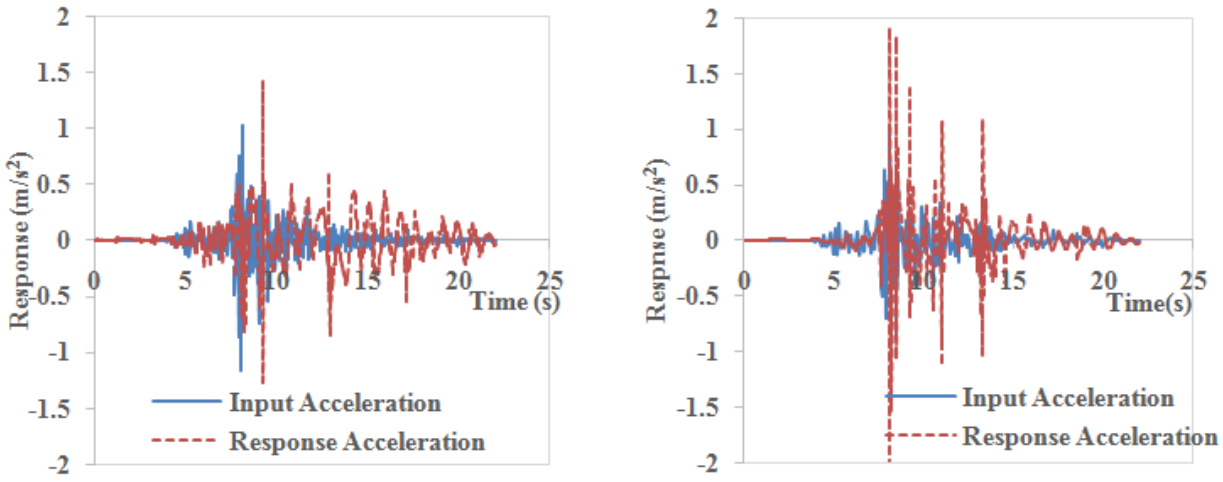

Figure 9: Acceleration response at pile head of diameter 0.6 m and 0.8 m piles, respectively, with dynamic time under kinematic interaction

3.2 Embedment Depth Effect

The lateral deformation of the pile at different depths for both pile diameters under consideration are shown in Figure 10. The lateral displacement of the pile decreases with increasing embedment depth, due to the increasing soil stiffness with dept. The bending moment diagram along the pile length is shown in Figure 11 for both pile diameters. The maximum bending moment is attained at the bottom of the pile. The pile diameter affects the amplitude of the bending moments close to the bottom of pile, the higher moment being exhibited for the larger pile diameter, due to the increased stiffness. The patterns of bending moment under dynamic load for both diameters are the same and this result is similar to previous literature [33].

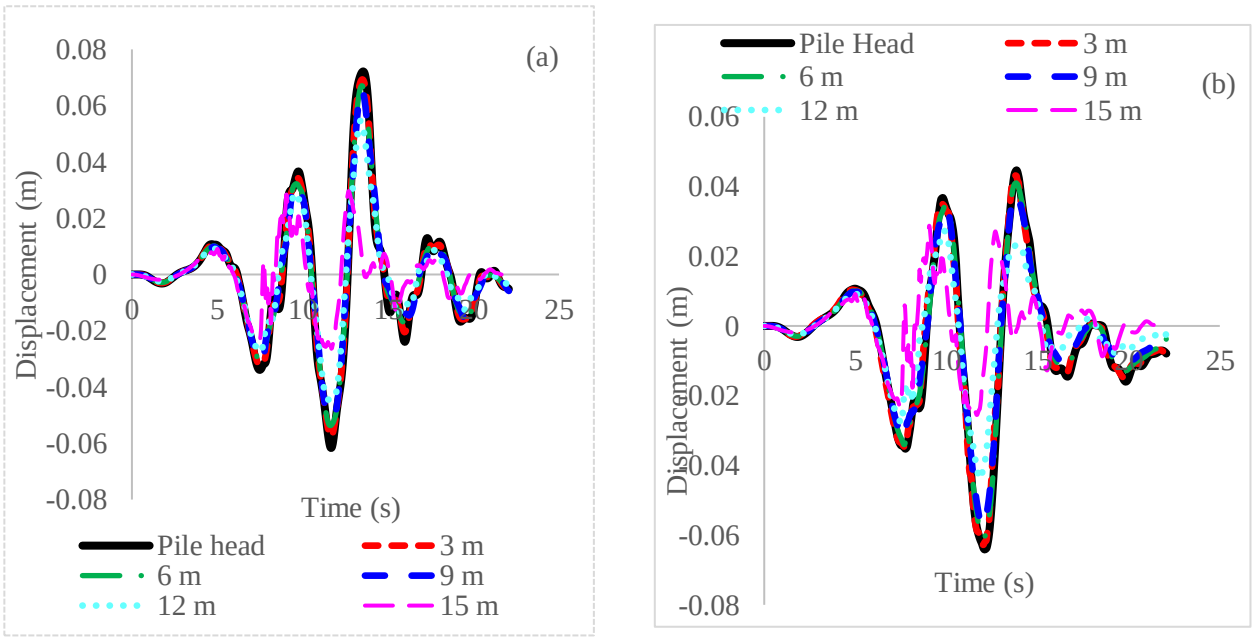

Figure 10.Lateral displacement under kinematic interaction a) for diameter 0.6 m pile b) for diameter 0.8 m pile

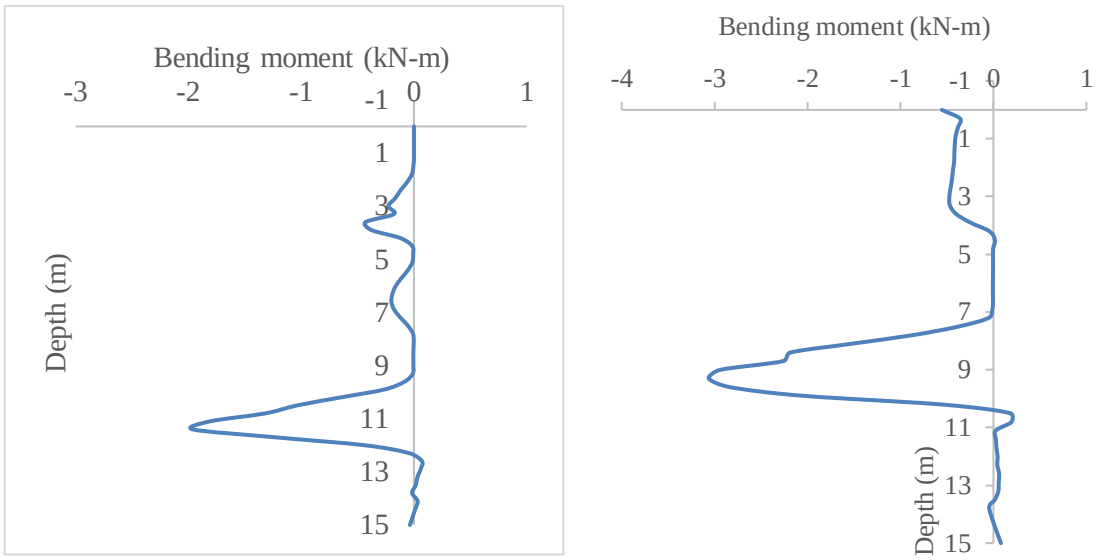

Figure 11: Bending moment along the pile length a) Diameter 0.6 m b) Diameter 0.8 m

4. CONCLUSIONS

During ground shaking, pile foundations are subjected to lateral forces. Even though the primary function of a pile foundation is to carry vertical loads from the superstructure, it has to withstand lateral forces due to seismic actions. The seismic response of the soil is affected by an interaction between the structure and surrounding soil.

In this research, seismic hazard analysis for the specified electric converter station area was carried out. Probabilistic seismic hazard analysis has been carried out for design basis earthquake, corresponding to 475 years of return period and its peak ground acceleration is determined to be 0.13g that falls in the range of PGA values determined by previous researchers.

The response of the pile under seismic load in layered soil has been carried out by employing finite element analysis software ABAQUS. The dynamic analyses results by considering plain concrete sections of the pile showed that the displacement of the pile is not within permissible ranges of the literature, which calls for further detailed analyses. Otherwise the use of the smaller diameter pile shall be disregarded, as the calculated displacement is more than twice the allowable. Qualitatively, the results of current investigation are in good agreement with the findings of previous researches and theoretical expectations.

REFERENCES

[1] Hongnan, L. and Haifeng, B. 2006. High Voltage transmission tower line system subjected to disaster loads. Progress in Natural Science, 16(9) 899-911.

[2] Hall, F. J., Holmes, T. W. and Somers, P. 1994. The Northridge, California Earthquake of January 17: General Reconnaissance Report., University at Buffalo.

[3] Ballantyne, D., Borcherdt, R.D. and Ed. Shinozuka, M. 1995. The Hanshin-Awaji Earthquake of January 17, 1995: Performance of lifelines. US National Center for Earthquake Engineering Research (NCEER).

[4] Zhang, P., Song, G., H.N., Li and Lin, Y. X.2013. Seismic Control of Power Transmission TowerUsing Pounding TMD. 10, s.l. : Journal of Engineering Mechanics, ASCE, 139(10) 51-54.

[5] Liu, C., Mao, L., Wang, C.; Zha, C.2016.Seismic Performance Research of Transmission Tower in Consideration of the Pile-soil-structure System. IOP Confneference Series, Singapore.

[6] Herbert, S. 2013. Assessing seismic risk in Ethiopia. Birmingham : University of Birmingham, GSDRC Helpdesk Research Report 1087.

[7] Bell, F.G. 2003. Geological Hazards-Their Assessment, Avoidance and Mitigation, CRC Press.

[8] Poulos, H G. 2013. Practical approaches to seismic design of deep foundations. Proc.

19th NZGS Geotechnical Symposium, [ed.] C.Y. Chin. Queenstown.

[9] Novak, M. 1974, Practical approaches to seismic design of deep foundations. Canadian Geotechnical Journal, 11(4) 574-598.

[10] Bentley, K. J. and Naggar, M. H., 2000, Numerical Analysis of Kinematic Response of Single Piles.Canadian Geotechnical Journal, 37(6) 1368-1382.

[11] Maheshwari, B., Truman, K. El Naggar, M. and Gould, P., 2004. Three-dimensional finite element nonlinear dynamic analysis of pile groups for lateral transient and seismic excitations.Canadian Geotechnical Journal 41(1) 118-133.

[12] Dongmei, C. and Truman, K. Z.2004.Effects of Pile Foundation Configirationin in Seismic Soil-Pile-Structure Interaction. 13th World Conference on Earthquake Engineering, Vancouver, B.C., Canada.

[13] Gebregziabher, H. F. and Assefa, T. 2021. Simplified Full Dynamic Analysis of a Railway Tunnel in Ethiopia. World Journal of Engineering and Technology, 9(3) 444-457.

[14] Baker, J. W., Bradley, B. A., and Stafford, P. J.2015.An Introduction to Probabilistic Seismic Hazard Analysis (PSHA). Cambridge : Cambridge University Press.

[15] Ayele, A. 2017. Probabilistic seismic hazard analysis (PSHA) for Ethiopia and neighboring region. Journal of African Earth Sciences, Elsevier, , Journal of African Earth Sciences, 134, 257-264.

[16] Kaklamanos, J. and Baise, L. G. Boore, D. M. 2011. Estimating Unknown Input Parameters when Implementing the NGA Ground-Motion Prediction Equations in Engineering Practice. Earthquake Spectra, 27(4)1219–1235.

[17] Wells, D. L. and Coppersmith, K. J. 1994. New empirical relationships among magnitude rupture length, rupture width, rupture area, and surface displacement. Bulletin of the Seismological Society of America 84(4) 974–1002.

[18] Bommer, J. J., Douglas, J. and Strasser, F. O. 2003. Style of Faulting in Ground Motion Prediction Equiations. Bulletin of Earthquake Engineering, 1, 171-203.

[19] Chiou, B. and Youngs, R. R. 2008. An NGA model for the average horizontal component of peak ground motion and response spectra. Earthquake Spectra 24(1) 173-216.

[20] Martin, J. and Perez, C. J. 2009. Application of a generalized lognormal distribution to engineering data fitting. [ed.] S. Martorell, Guedes Soares C. and J. Barnett. Safety, Reliabilitty and Risk Analysis. s.l. : Taylor and Francis.

[21] Huyse, L., Chen, R. and Stamatakos, J. A., 2010. Application of Generalized Pareto Distribution to Constrain Uncertainty in Peak Ground Accelerations. Bulletin of Seismological Society of America 100(1), pp. 87-101.

[22] Worku, A.2011.Recent Developments in the definitions of design earthquake ground motion. Zede Journal of EEA, 28(l), 1-15.

[23] Bazzurro, P., Cornell, C. A. 1999. Disaggregation of Seismic Hazard. Bulletin of the seismological society of America 89(2) 501-520.

[24] McGuire, R. K. 1995. Probabilistic seismic hazard analysis and design earthquakes: Closing the loop. Bulletin of the Seismological Society of America, Vol. 85(5)1275-1284.

[25] Baker, J. W. 2007. Measuring Bias in Structural Response Caused by Grand Motion Scaling. 8th Pacific Conference on Earthquake Engineering,5-7 Decemnber 2007, Singapore.

[26] Lin, T. , Baker, J. 2011. Probabilistic seismic hazard deaggregation of ground motion prediction models. Proceedings of the 5thInternational Conference on Earthquake Geotechnical Engineering, 9-14 Jan. 2011, Santiago, Chile.

[27] Kwon, S.Y., Yoo, M. 2019. Evaluation of Dynamic Soil-Pile-Structure Interactive Behavior in Dry Sand by 3D Numerical Simulation. Applied Sciences 9(13) 2612.

[28] Balendra, S. 2005. Numerical Modeling of Dynamic Soil-Pile-Structure Interaction. MSc Thesis. Washington, USA : Washington Sate University.

[29] Jeremic, B., Jie, G. Preisig, M., Tafazzoli, N. 2005.Time domain simulation of soil–foundation–structure interaction in non-uniform soils.. The Journal of the Intenational Association for Earthquake Engineering, Nonlinear Finite Element Analysis of Dynamic Soil-Foundation-Structure Interaction. 38(5) 699-715.

[30] Lysmer, J., Kuhlemeyer, R. L., 1969. Finite dynamic model for infinite media.Journal of the Engineering Mechanics Division,

ASCE, , Journal of the Engineering Mechanics Division 95(4) 859-877.

[31] Feng, L. B., Hong, H., Bi, K.M., Li, H.N.2011. Seismic Response Analysis of Transmission Tower-Line System on a Heterogeneous Site to Multi-Component Spatial Ground Motions., Advances in Structural Engineering 14(3), 457-474.

[32] Bouzid, D.A., Bhattacharya, S., Dash, S.R. 2013. Winkler spring (p-y curves) for pile design from stress-strain of soil : FE assesment of scaling coffiecents using the mobilized strength design. Geomechanics and Engineering 5(5) 379-399.

[33] Dezi, F., D, Carbonary, S., Leoni, G. 2009. Kinematic bending moment in pile foundation, Soil Dyanmics and Earthquake Engineering 30(3) 119-132.

All © 2023 are reserved by International Journal of Advanced Science and Engineering. This Journal is licensed under a Creative Commons Attribution-Non Commercial-ShareAlike 3.0 Unported License.